iScience

CellPress
OPEN ACCESS

Article

In-plane Assembly of Distinctive 2D MOFs with Optimum Supercapacitive Performance

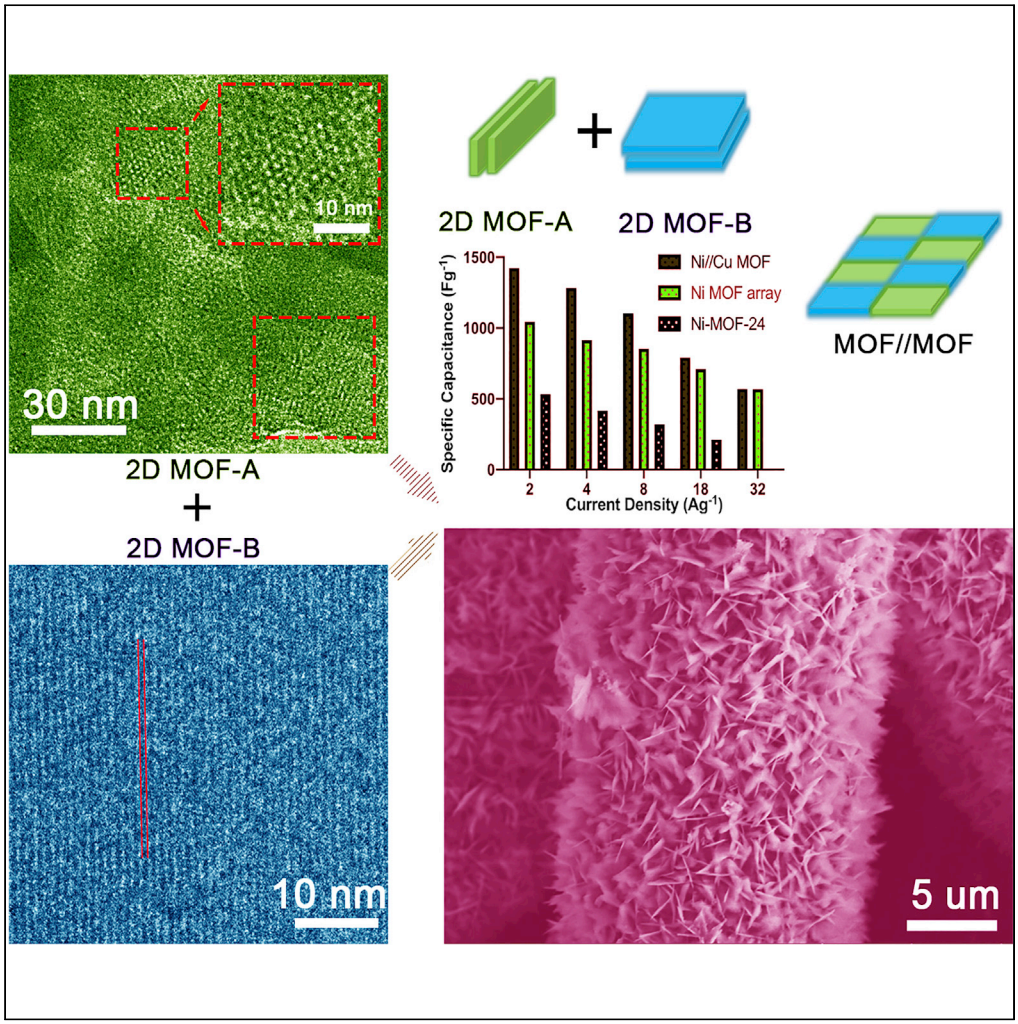

Ting Deng, Xiaoyuan Shi, Wei Zhang, Zizhun Wang, Weitao Zheng

weizhang@jlu.edu.cn (W.Z.)
wtzheng@jlu.edu.cn (W.Z.)

HIGHLIGHTS

Two kinds of 2D MOFs are successfully in-plane composited

Distinctive MOFs with specific functions are integrated into one homogeneous layered MOF

Maximum energy density and power density can reach 57 Wh kg^{-1} and 48,000 W kg^{-1}

Deng et al., iScience 23, 101220
June 26, 2020
https://doi.org/10.1016/j.isci.2020.101220

iScience

CellPress
OPEN ACCESS

Article

In-plane Assembly of Distinctive 2D MOFs with Optimum Supercapacitive Performance

Ting Deng,[1] Xiaoyuan Shi,[2] Wei Zhang,[1,3,4,5,*] Zizhun Wang,[1] and Weitao Zheng[1,*]

SUMMARY

2D metal organic frameworks (MOFs) with layered structure and much exposed atoms on the surface are expected to be promising electrode materials for hybrid supercapacitors. However, the insulating character strongly hinders their further applications. Herein, we propose a novel MOF//MOF strategy to enhance 2D MOF's conductivity, by which two kinds of 2D MOFs with specific functions are concurrently incorporated into one homogeneous layered MOF with enhanced conductivity and electrochemical performance. The synthesized Ni//Cu MOF shows a triple high capacitance of 1,424 Fg^{-1} and excellent rate capability compared with the pristine Ni MOF. A hybrid supercapacitor is thereof fabricated, which can provide a maximum energy density of 57 Wh kg^{-1} and a maximum power density of 48,000 W kg^{-1}. These results not only demonstrate that our strategy can effectively boost the conductivity and redox activity but also pave new routes to synthesize new MOFs for various applications.

INTRODUCTION

Metal organic frameworks (MOFs) bridged by metal ions and organic linkers display a high flexibility of geometry, composition and functionality, resulting in the versatility in diverse applications (Furukawa et al., 2013; Li and Xu, 2013). Especially, two-dimensional (2D) MOFs with much exposed atoms on the surface show great potentials in energy storage devices (ESDs), such as hybrid supercapacitor, which is expected to deliver a considerable energy density compared with batteries while preserving the excellent power density of supercapacitors (Duan et al., 2019; Nam et al., 2019; Wang et al., 2016; Yuan et al., 2019).

Nevertheless, the insulating character of MOF has prevented them from emerging as popular candidate materials for ESDs (Talin et al., 2014). Accordingly, much efforts have been devoted to improving MOF's conductivity (Bhardwaj et al., 2018). One commonest way is to composite MOF with conductive materials, such as carbon materials (Wei et al., 2017) and conductive polymers (Wang et al., 2015). When it comes to 2D MOFs, in-plane composition with conductive additive is much desirable, otherwise the counterpart material such as graphene may cover or even seal the interlayer spacing for electrolyte diffusion, thus resulting in the uncertainty of electrochemical performance (Sun et al., 2017; Yoo et al., 2011). Another popular method is synthesizing conducting MOFs, which are also successfully demonstrated as the electrode material for supercapacitor (Li et al., 2017; Sheberla et al., 2017; Zhou et al., 2019). With a close scrutiny at their electrochemical performance, one can see that their cyclic voltammetry (CV) curves are rectangle, indicating the electronic double-layer capacitance (EDLC) (Conway, 1999). Once metal ions are fully chelated with organic ligands, neither energy pathways nor free charge carriers are present. As a result, it usually renders these potential active sites electrochemically inactive or inert, leading to a limited capacitance toward high energy density in hybrid supercapacitor. In addition, the cost of conducting MOF is quite expensive, which in turn endows a low price/performance ratio of pure conducting MOF in supercapacitor industrialization. Therefore, creating one easily manipulated and cost-effective strategy to boost 2D MOF's conductivity and modifying their electrochemical performance for future high-performance hybrid supercapacitor is of great significance.

Synthesizing core-shell MOF structure is one popular means to merge multiple functions of different 3D MOFs together to one unit for optimizing utilization (Lee et al., 2020; Zhang et al., 2018). Inspired by that, due to the flexibility of MOF constituent we propose a novel MOF//MOF strategy, in which two kinds of 2D MOFs with specific functions (high conductivity and high electrochemical activity) are concurrently incorporated into one homogeneous layered MOF with enhanced conductivity and electrochemical

[1]Key Laboratory of Mobile Materials MOE, School of Materials Science & Engineering, Electron Microscopy Center, and International Center of Future Science, Jilin University, Changchun 130012, China

[2]Key Laboratory of Polyoxometalate Science of Ministry of Education, Northeast Normal University, Changchun 130024, China

[3]Wuhan National Laboratory for Optoelectronics, Huazhong University of Science and Technology, Wuhan 430074, China

[4]IKERBASQUE, Basque Foundation for Science, Bilbao 48013, Spain

[5]Lead Contact

*Correspondence: weizhang@jlu.edu.cn (W.Z.), wtzheng@jlu.edu.cn (W.Z.)

https://doi.org/10.1016/j.isci.2020.101220

performance for hybrid supercapacitors. Herein based on our previous work using $Co(OH)_2$ as both the precursor and the template, we have successfully integrated two-layered MOFs into one homogeneous, oriented 2D MOF array, which shows further substantial electrochemical performance promotion (Deng et al., 2018). One component is Ni-MOF-24, which serves as the electrochemically active unit, and the other MOF is $Cu_3(HITP)_2$ (HITP = 2,3,6,7,10,11-hexaiminotriphenylene) functioning as the conducting unit to activate adjacent Ni-MOF-24. Correspondingly, Ni-MOF-24//$Cu_3(HITP)_2$ (Ni//Cu MOF) array shows a high specific capacitance of 1,424 Fg^{-1} at the current density of 2 Ag^{-1}, which is almost three-fold of Ni-MOF-24, and retains 570 Fg^{-1} at the current density of 32 Ag^{-1}. Based on the high capacitance and excellent rate capability, a hybrid supercapacitor is thereof fabricated, which can deliver a maximum energy density of 57 Wh kg^{-1} and a maximum power density of 48,000 W kg^{-1}. In addition, this hybrid supercapacitor exhibits the capability of fast charging to elongate the endurance in a short time. The energy density retains 97%, 95%, 82%, 79%, and 53% of the maximum energy density when it is charged at 2, 4, 8, 16, and 32 Ag^{-1} and discharges at 1 Ag^{-1}, respectively. Such promising electrochemical performances strongly demonstrate that MOF//MOF strategy originated from MOF tunable composition is capable to promote 2D MOF's performance in ESDs, which now renders MOF to be a competitive electrode material in all aspects.

RESULTS

In the typical method (Figure 1A) MOF core-shell structure can be obtained through the introduction of one MOF to the precursors of another, by which we can integrate the functions of two MOFs into one unit. When it comes to 2D MOFs for ESDs, this simple coating strategy may not only impede the electrolyte diffusion but also deteriorate the insulating situation. In a jigsaw puzzle, each tiny 2D piece is indispensable to the final image. Converse thinking, however, we select two 2D MOFs with different functions and concurrently forge them into a homogeneous MOF, which is quite similar to working out a puzzle (Figure 1B). In this strategy, one MOF we select is Ni-MOF-24, which shows a disoriented layered morphology by using scanning electron microscopy (SEM) (Figure 1C). The lattice parameters *a*, *b*, and *c* of Ni-MOF-24 are 10.2, 8.0, and 6.3 Å, respectively. With a high-resolution transmission electron microscopy (HRTEM, Figure 1D), one can see the largest exposed facet is (100) plane, and the lattice fringe is calculated to be 1.06 nm. Many reports have demonstrated the electrochemical activity of Ni-MOF-24, and enhancing the conductivity by compositing with carbon fibers (CFs) can upgrade its electrochemical performance for supercapacitor (Wen et al., 2015; Yang et al., 2014a; Yang et al., 2014b). But this method only engineers the conductivity from outside, which ignores its intrinsic conductivity. Herein, the other component we chose is a conducting MOF, $Cu_3(HITP)_2$, which shows a submicron crystal size (Figure 1E). $Cu_3(HITP)_2$ is also a 2D MOF with layered structure (Figure 1F), and the inset HRTEM image clearly displays a honeycomb-shaped pore structure along *c* axis, which presents a perfect hexagonal arrangement of atoms with unit cell parameters of $a = b =$ 22.3 Å and $c = 6.6$ Å (Figure S1). The lattice fringe of the most exposed facet was calculated to be 0.92 nm (Figure S2), which corresponds to the d_{100}-spacing and agrees with the XRD pattern. $Co(OH)_2$ is utilized as the precursor and template (Figure 1G) to successfully synthesize Ni//Cu MOF array on carbon fiber papers (CFPs) (Figure 1H) (Deng et al., 2018). Figure 1I shows the X-ray diffraction (XRD) patterns of Ni//Cu MOF and $Cu_3(HITP)_2$. At ~5°, Ni//Cu MOF shows a new peak that belongs to $Cu_3(HITP)_2$ (circled highlighting), whereas the peak at ~27 degrees of $Cu_3(HITP)_2$ disappears, indicating the successful in-plane composition of two units into one 2D MOF (Figure S3). The similar *c* parameters of $Cu_3(HITP)_2$ and Ni-MOF-24 may facilitate the in-plane composition process.

To acquire further details of Ni//Cu MOF structure, high-angle annular dark-field scanning transmission electron microscopy (HAADF-STEM) is conducted and elemental distribution of Ni//Cu MOF is probed by energy dispersive X-ray spectroscopy (EDS) (Figure 2A). As we can see that Ni, Co, Cu, and elements from ligands (Figure S4) are evenly distributed in Ni//Cu MOF, indicating the homogeneity of MOF. Figure S5 shows contents of these elements. The content of Ni is dominant, which mainly contribute to capacitance. As proved by our previous work, the weak intensity is due to small content of Co because of which $Co(OH)_2$ sacrifices itself as the precursor to react and induce MOF growth in the assembly. Because $Co(OH)_2$ is an amphoteric hydroxide, it can react with p-benzenedicarboxylic (PTA) linkers. So during the formation of MOF array, $Co(OH)_2$ react with PTA concurrently, which leads to a less content of Co species in the final product (Deng et al., 2018). A small dose of $Cu(NO)_3$ is added into the precursor solution so that the content of Cu is also low. To clarify the surface states of Ni//Cu MOF, X-ray photoelectron spectroscopy (XPS) is exploited (Figures 2B–2D). Figure 2B shows Ni 2*p* XPS spectrum, which can be decomposed into two components centered at 856.2 and 873.7 eV, typically indicating the valence of Ni species is +2 (Guan et al., 2017; Li et al., 2013). In the XPS spectrum of Co, the binding energies for $2p_{3/2}$, $2p_{1/2}$, and corresponding satellite structures are at 780.3, 794.3, 786.5, and 803.9 eV, respectively (Figure 2C). In the fitted curve of Co species of Ni//Cu MOF, the main peak Co $2p_{3/2}$ is detected at 779.6 eV, implying the valence of Co is

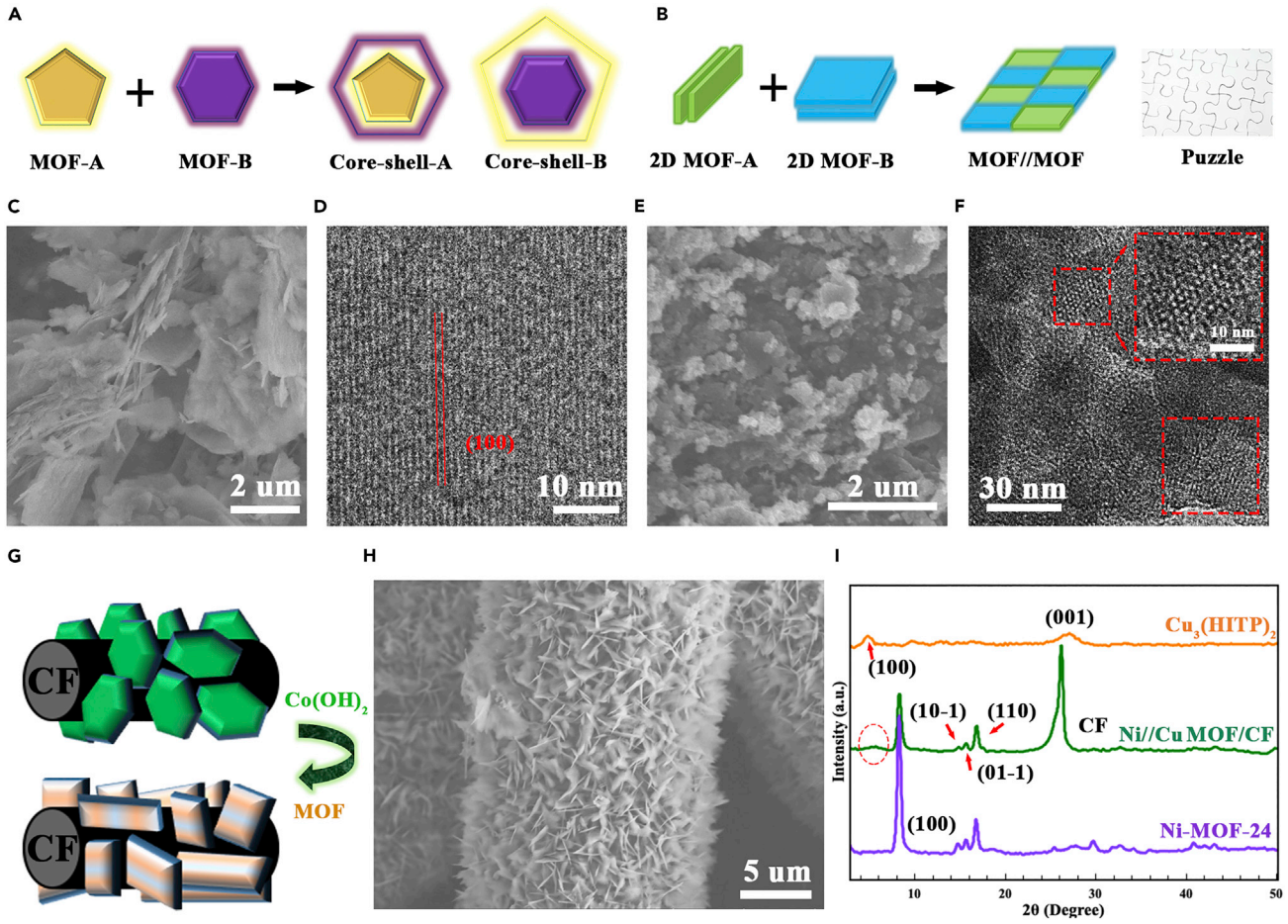

Figure 1. The Schematic Illustration of MOF//MOF Synthesis and Physical Characterization

(A) Core-shell structure synthesis route.

(B) MOF//MOF synthesis illustration.

(C) SEM image of Ni-MOF-24. (D) HRTEM image of Ni-MOF-24.

(E) SEM image of $Cu_3(HITP)_2$. (F) HRTEM image of $Cu_3(HITP)_2$. In the red boxes the honeycomb-shaped pore structure and lattice fringe can be seen (as the feature is very sensitive to the electron beam in TEM, we applied both largely reduced beam intensity and extremely short acquiring time).

(G) MOF//MOF array synthesis. $Co(OH)_2$ is used as both template and precursor for preparation.

(H) SEM image of Ni//Cu MOF array on CF.

(I) XRD patterns of Ni-MOF-24, $Cu_3(HITP)_2$, and Ni//Cu MOF array on carbon fiber (CF).

mainly +3 and also the fact that $Co(OH)_2$ not only serves as the template but also participates in MOF assembly (Biesinger et al., 2011; Grace Victoria and Moses Ezhil Raj, 2018). Cu $2p_{3/2}$ and $2p_{1/2}$ are detected at 934.5 and 954.5 eV, respectively. The main peak of Cu $2p_{3/2}$ locates at 935 eV in the fitted curve, which is the characteristics of Cu^{2+} (Figure 2D) (Biesinger et al., 2010). The XPS spectrum of N element can be decomposed into three components (Figure S6), within which the main peak locates at 400.1 eV. This is the evidence that N species have chelated with metal ions, proving the existence of HITP in the structure (Zhang et al., 2017). According to Fourier transform infrared (FT-IR) spectra (Figure 2E), there is a broad band at 3,435 cm^{-1} due to O-H stretching mode of hydroxyl group in Ni-MOF-24. Two sharp peaks at 1,382 and 1,584 cm^{-1} are related to COO vibration, whereas the peaks stand for out-of-plane ring bending vibration are detected at around 800 cm^{-1}. Compared with Ni-MOF-24, there is also a wide peak centered around 3,400 cm^{-1}, which is responsible for amino-group of $Cu_3(HITP)_2$. Peaks from 1,200 to 1,600 cm^{-1} are the characteristic of C=N stretching vibrations. After the composition of these two 2D MOFs, there is a shoulder peak at 1,602 cm^{-1} due to C=N stretching beside the sharp peak of COO vibration (1,584 cm^{-1}), indicating the existence of HITP and PTA linkers in the structure. Figure 2F portrays the Raman spectra of Ni-MOF-24, $Cu_3(HITP)_2$, and Ni//Cu MOF. In the curve of Ni-MOF-24 the sharp peaks at 1,251 and 1,436 cm^{-1}

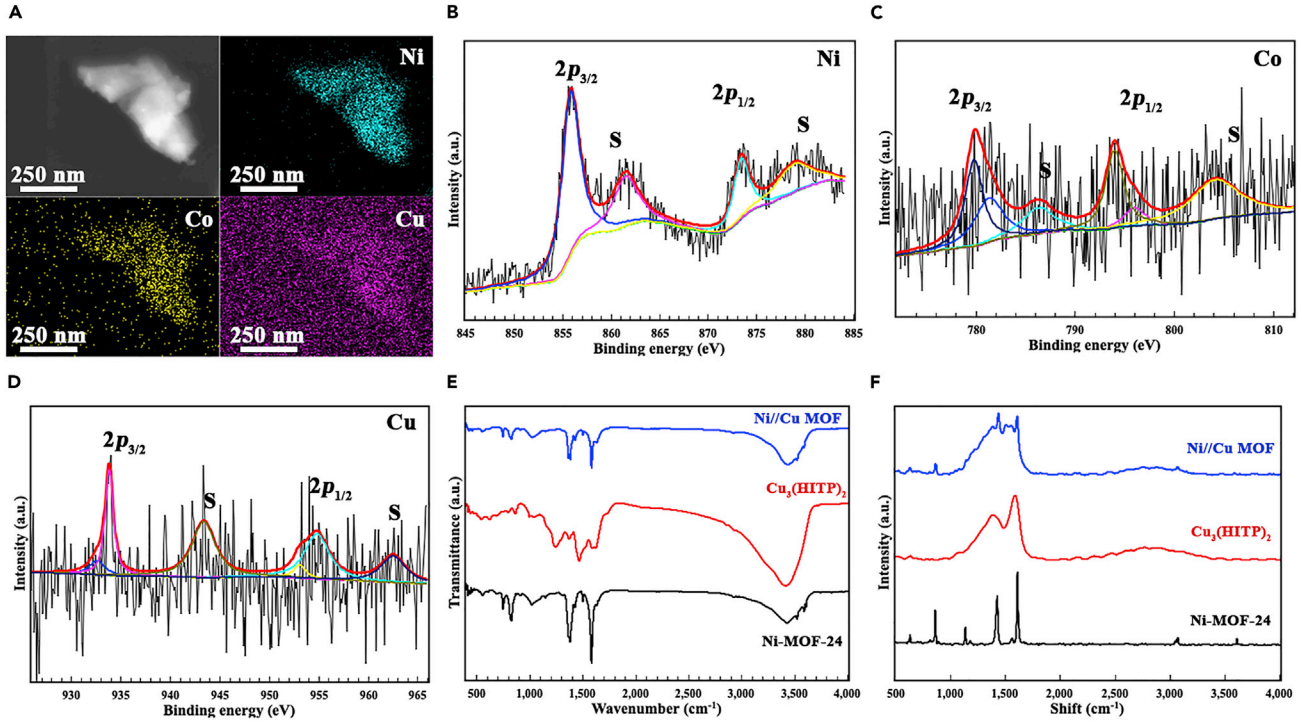

Figure 2. STEM-EDS Analysis and XPS Spectra of Ni//Cu MOF

(A) STEM image and EDS elemental mapping of Ni//Cu MOF.

(B) XPS spectrum of Ni 2*p*. (C) XPS spectrum of Co 2*p*. (D) XPS spectrum of Cu 2*p*

(E) FT-IR spectra of Ni-MOF-24, $Cu_3(HITP)_2$, and Ni//Cu MOF. (F) Raman spectra of Ni_MOF-24, $Cu_3(HITP)_2$ and Ni//Cu MOF, respectively.

are due to COO vibration mode, whereas the peak at 1,622 cm^{-1} is caused by C=C of benzene rings. The peak at 793 cm^{-1} indicates the C-H bending. Besides the peak for C=C, there is a wide band centered at 1,464 cm^{-1}, which is related to C=N bond in $Cu_3(HITP)_2$. Accordingly, the feature peaks of each component are presented in Ni//Cu MOF, indicating the successful composition of these two MOFs. The specific surface area (SSA) of Ni//Cu MOF and Ni-MOF-24 is evaluated because it is an important factor that can influence the overall performance (Figure S7). After the in-plane composition of conductive MOF, an increased SSA (90 m^2g^{-1}) is obtained on the basis of an originally small SSA (26 m^2g^{-1}), which is a good sign for electrochemical performance of Ni//Cu MOF.

To identify the electrochemical properties of Ni//Cu MOF array, it has been tested as the active material in 1 M KOH electrolyte, and a saturated calomel electrode (SCE) is used as the reference electrode. Figure 3A shows the cyclic voltammetry (CV) curves of Ni//Cu MOF array, Ni-MOF-24, and $Co(OH)_2$ collected at the scan rate of 10 mVs^{-1}. There is one pair of redox peaks in each CV curve proving their battery-mimic mechanism (Deng et al., 2017; Simon et al., 2014). The redox peaks of Ni//Cu MOF appear at higher potential regions than $Co(OH)_2$, as Ni^{2+}/Ni^{3+} species is active in the redox reaction rather than the mutual conversion between Co^{2+} and Co^{3+} (Deng et al., 2017; Li et al., 2013). This process could be represented by the following equation (Cao et al., 2019; Yang et al., 2020):

$$[Ni_3(OH)_2(C_8H_4O_4)_2\cdot(H_2O)_4]\cdot 2H_2O + OH^- - e^- \leftarrow\rightarrow [Ni_3O(OH)(C_8H_4O_4)_2\cdot(H_2O)_4]\cdot 2H_2O + H_2O.$$

Through H^+ intercalation/de-intercalation, the CV curve of Ni//Cu MOF array shows the characteristic of battery-type materials. When it is compared with CV curve of Ni-MOF-24, higher peak current and larger CV area imply higher redox activity of Ni//Cu MOF than Ni-MOF-24. The CV curve of pure $Cu_3(HITP)_2$ is a line, suggesting that $Cu_3(HITP)_2$ nearly shows no capacitance (Figure S8). The specific capacitance of Ni//Cu MOF array, Ni-MOF-24, and $Co(OH)_2$ are calculated to be 1,424, 517, and 289 Fg^{-1} at the current density of 2 Ag^{-1}, respectively (Figure 3B). The capacitance of Ni//Cu MOF is almost triple high of pure Ni-MOF-24. In addition, Ni//Cu MOF displays excellent capability, whose capacitance can reach 1,424, 1,284, 1,103, 792, and 570 Fg^{-1} at the current

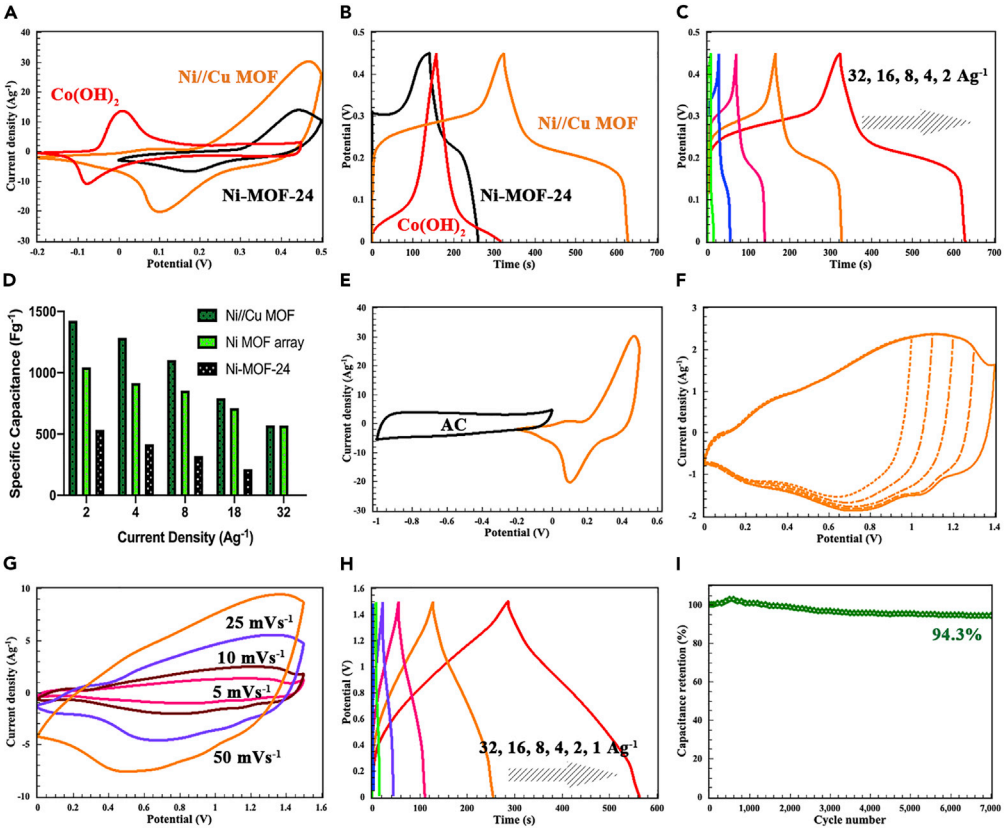

Figure 3. Electrochemical Evaluation of Ni//Cu MOF and Corresponding Hybrid Supercapacitor

(A) The CV curve of Ni//Cu MOF, Ni-MOF-24 and $Co(OH)_2$ collected at the scan rate of 10 mVs^{-1}.

(B) Galvanostatic profiles of Ni//Cu MOF, Ni-MOF-24, and $Co(OH)_2$ at the current density of 2 Ag^{-1}, and the capacitance can reach 1,472; 533; and 688 Fg^{-1}, respectively.

(C) Galvanostatic profiles of Ni//Cu MOF at various current densities.

(D) The capacitance comparison of Ni//Cu MOF, Ni MOF array, and powder Ni-MOF-24 at all current densities.

(E) CV curves of Ni//Cu MOF and AC at the scan rate of 10 mVs^{-1}.

(F) CV curves of hybrid supercapacitor with different potential windows.

(G) CV curves at different scan rates, ranging from 5 to 50 mVs^{-1}.

(H) Galvanostatic profiles collected at various current densities.

(I) The stability test of the capacitor. After 7,000 cycles, the capacitance holds a 94.3% retention of its initial capacitance.

density of 2, 4, 8, 16, and 32 Ag^{-1}, respectively (Figure 3C). Ni//Cu MOF not only shows improved specific capacitance at all current densities than Ni-MOF-24 in powder form but also excels when compared with Ni-MOF array (Figure 3D). To investigate the conductivity, we directly measure the resistance of Ni-MOF-24 array on CFP and Ni//Cu MOF array on CFP at room temperature. The resistance of Ni-MOF-24 is 0.48 ohm, and the number for Ni//Cu MOF is reduced to 0.21 ohm. Both Ni//Cu and Ni-MOF arrays use $Co(OH)_2$ as the precursor and template, resulting in a small Co content in their constituents. But after the successful in-plane composition of conductive 2D MOF with Ni-MOF-24, substantial electrochemical performance promotion is shown by Ni//Cu MOF array, which further proves the importance of intrinsic conductivity. In addition, we also test the stability of Ni//Cu MOF array. As we can see in Figure S9, after 7,000 charge/discharge cycles, the peaks indexed to (100) of Cu_3(HITP)$_2$ and (100) of Ni-MOF-24 show no obvious shifts, which implies the structural stability of Ni//Cu MOF array. A hybrid supercapacitor is fabricated, which involves Ni//Cu MOF array, active carbon (AC), and 1 M KOH solution as the positive electrode, negative electrode, and electrolyte, respectively (Figure 3E). Figure 3F presents CV curves of this capacitor collected at 10 mVs^{-1} while in different operation window. The voltage window can reach 1.5 V, and the CV curves show no obvious deformation at different scan rates ranging from 5 to 50 mVs^{-1} (Figure 3G), indicating the excellent rate capability of this capacitor. Figure 3H shows the charge/discharge profiles at various current densities (Figure 3H). This hybrid capacitor can deliver a maximum energy density of 57 Wh kg^{-1} at a power density of 1500 W kg^{-1} at 1 Ag^{-1} and a maximum power density of 48,000 W kg^{-1} while the energy

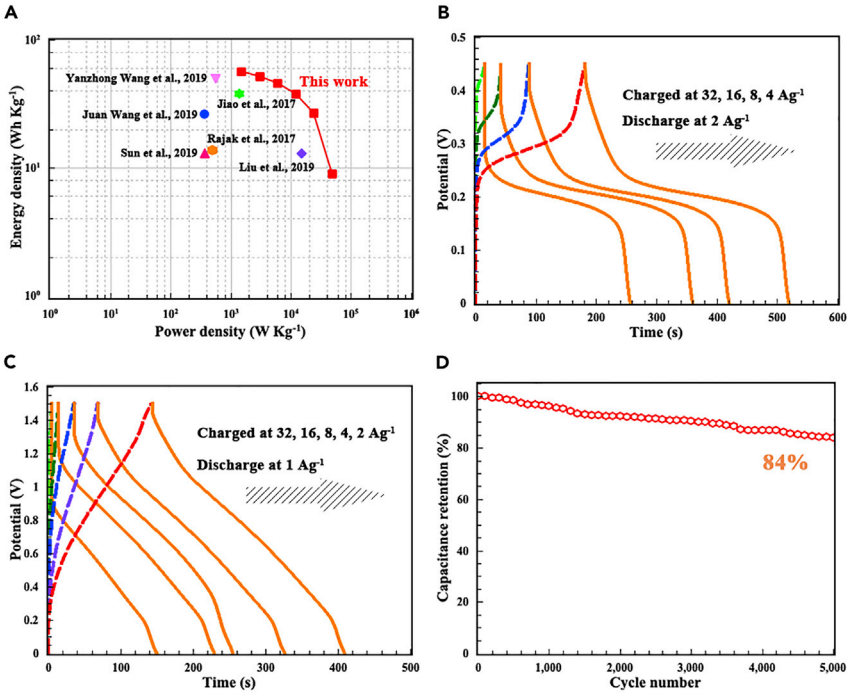

Figure 4. The Electrochemical Performance of Hybrid Supercapacitor

(A) Ragone plots regarding power density to energy density.

(B) Fast charging test of Ni//Cu MOF electrode at different charging current densities.

(C) Fast charging test of hybrid supercapacitor at different charging current densities.

(D) The cyclability of hybrid supercapacitor under fast charging condition (charging at 8 Ag^{-1}, discharge at 1 Ag^{-1}). After 5,000 cycles, 16% decay is observed.

density remains 9 Wh kg^{-1} at 32 Ag^{-1}. A remarkable long-term cyclability of this hybrid capacitor is also reached, and only 5.7% decay of its initial capacitance is observed after 7,000 cycles (Figure 3I).

According to the charge/discharge profile, the energy densities and the corresponding power densities this hybrid supercapacitor can deliver at the same time are displayed in the Ragone plot (Figure 4A), which is higher than other recently pure MOF-based aqueous supercapacitors (Jiao et al., 2017; Liu et al., 2019; Rajak et al., 2017; Sun et al., 2019; Wang et al., 2019a, 2019b; Wen et al., 2015). In our MOF//MOF strategy the incorporated conductive part $Cu_3(HITP)_2$ motivates Ni-MOF-24 in their neighborhood to be electrochemically active for capacitance contribution. Thus, the capacitance of Ni//Cu MOF is almost triple high of pure Ni-MOF-24, which is further enhanced in comparison with Ni-MOF array and indicates increasing the intrinsic conductivity can further optimize its electrochemical performance. On the other hand, the imbedded $Cu_3(HITP)_2$ builds up highways for electron transfer by increasing MOF conductivity, which enables this MOF-based device with fast response to large current densities and a particularly high power density of 48,000 W kg^{-1}. Moreover, due to the fact that numerous portable electronic devices have simplified daily life, long endurance and fast charging ability are of considerable significance (Severson et al., 2019). Figure 4B shows the charge/discharge profiles of Ni//Cu MOF array, in which Ni//Cu MOF discharges at the current density of 2 Ag^{-1} and is charged at the current densities of 4, 8, 16, and 32 Ag^{-1}, respectively. The capacitance can reach 1,354, 1,248, 1,184, and 832 Fg^{-1}, respectively. In addition, the hybrid supercapacitor discharges at the current density of 1 Ag^{-1} and is charged at 2, 4, 8, 16, and 32 Ag^{-1}, respectively (Figure 4C). The energy density can hold 97%, 95%, 82%, 79%, and 53% of its maximum energy density in reduced charging time, suggesting its excellent rate capability as the potential of fast charging. After 5,000 fast charging cycles (charging at 8 Ag^{-1}, discharge at 1 Ag^{-1}) this hybrid supercapacitor still holds an 84% retention of initial capacity (Figure 4D). The conductive MOF component not only increases the intrinsic conductivity for electron transfer but also evenly distributes in the structure to motivate adjacent Ni^{2+} species in redox reaction, which enhances specific capacitance, rate capability of Ni//Cu MOF, energy density, and power density of the hybrid supercapacitor concurrently. Besides, this MOF

array well preserves the porous and oriented morphology of $Co(OH)_2$, which can facilitate ion diffusion and also provide the spacing to buffer the volumetric change.

To further show the applicability of MOF//MOF strategy, we also synthesized a Co-MOF and Co//Cu MOF in powder form. As we can see in the XRD pattern (Figure S10), Co//Cu MOF also shows the peak centered around 5°, which belongs to $Cu_3(HITP)_2$, whereas the peak at 27 degrees of $Cu_3(HITP)_2$ disappears, indicating the successful in-plane composition of two-layered MOFs. As for the electrochemical performance, the capacitance of Co//Cu MOF shows an almost triple high capacitance of pure Co-MOF, which is in accordance with Ni//Cu MOF (Figure S11). The outstanding electrochemical performances of Ni//Cu MOF and Co//Cu MOF give credits to MOF//MOF strategy we proposed to modify the electrochemical performance of 2D MOF by integrating distinctive components with specific functions into one homogeneous MOF. The low conductivity has been the shackle of 2D MOF to excel in hybrid ESDs, which require high capacitance and high rate capability for outputting substantial energy density and power density. Thus, our findings pave a new way for engineering MOF's conductivity and electrochemical performance and also sheds light on the great potential of MOF in next-generation hybrid ESDs.

DISCUSSION

To summarize, we propose a novel strategy to activate the electrochemical performance of 2D MOF by integrating distinctive components with specific functions into one homogeneous layered MOF array. The new 2D MOF retaining the original layered structure with enhanced conductivity shows a triple high capacitance and improved rate capability of the pristine Ni-MOF. The corresponding hybrid supercapacitor shows the promising potential to achieve substantial energy and power density, which is the evidence that our strategy, based on the flexibility of MOF, can effectively upgrade electrochemical performance in hybrid ESDs, and such rational and novel design of MOF may take a substantial step toward high-performance ESDs for future.

Limitations of the Study

We believe that this MOF//MOF strategy may open a novel way toward rational design of new 2D MOF with enhanced electrochemical performance for energy storage, which is only limited to 2D MOFs with similar structures. However, only three kinds of 2D MOFs are analyzed in this study and the investigations of more different kinds of 2D MOF combinations are lacking. Meanwhile, other layered materials such as graphene or MXenes suitable for this strategy to boost the performance of MOFs and the corresponding analysis are also lacking.

Resource Availability

Lead Contact

Wei Zhang weizhang@jlu.edu.cn.

Materials Availability

The materials that support the findings of this study are available from the corresponding authors upon reasonable request.

Data and Code Availability

The data that support the findings of this study are available from the corresponding authors upon reasonable request.

METHODS

All methods can be found in the accompanying Transparent Methods supplemental file.

SUPPLEMENTAL INFORMATION

Supplemental Information can be found online at https://doi.org/10.1016/j.isci.2020.101220.

ACKNOWLEDGMENTS

This research is financially supported by the National Natural Science Foundation of China (Nos. 51802110, 51932003, 51902050 and 51872115), 2019 Innovation-High-tech Industry Program of Jilin Province Development and Reform Commission (No. 2019C046-4), Young Talents Fund Project of Jilin Provincial Science and Technology Department (No. 20190103025JH), China Postdoctoral Science Foundation (2018M640281), National

Postdoctoral Program for Innovative Talents (BX20180116), 2020 International Cooperation Project of the Department of Science and Technology of Jilin Province (20200801001GH), program for the Development of Science and Technology of Jilin Province (20190201309JC), Jilin Province/Jilin University Co-Construction Project Funds for New Materials (SXGJSF2017-3, Branch-2/440050316A36), the Open Project Program of Wuhan National Laboratory for Optoelectronics (2018WNLOKF022), Program for JLU Science and Technology Innovative Research Team (JLUSTIRT, 2017TD-09), the Fundamental Research Funds for the Central Universities JLU, and "Double-First Class" Discipline for Materials Science & Engineering.

AUTHOR CONTRIBUTIONS

T.D., X.Y.S., W.Z., and W.T.Z. conceived the idea and coordinated the study and led writing of the manuscript; Z.Z.W and W.Z. contributed to microscopy characterization and analysis; T.D. and X.Y.S contributed to electrochemical test and analysis; T.D. contributed to the rest physical characterizations and analysis. All co-authors discussed the results and made comments on the manuscript.

DECLARATION OF INTERESTS

The authors declare no competing interests.

Received: March 4, 2020
Revised: April 24, 2020
Accepted: May 27, 2020
Published: June 26, 2020

REFERENCES

Bhardwaj, S.K., Bhardwaj, N., Kaur, R., Mehta, J., Sharma, A.L., Kim, K.-H., and Deep, A. (2018). An overview of different strategies to introduce conductivity in metal–organic frameworks and miscellaneous applications thereof. J. Mater. Chem. A *6*, 14992–15009.

Biesinger, M.C., Lau, L.W.M., Gerson, A.R., and Smart, R.S.C. (2010). Resolving surface chemical states in XPS analysis of first row transition metals, oxides and hydroxides: Sc, Ti, V, Cu and Zn. Appl. Surf. Sci. *257*, 887–898.

Biesinger, M.C., Payne, B.P., Grosvenor, A.P., Lau, L.W.M., Gerson, A.R., and Smart, R.S. (2011). Resolving surface chemical states in XPS analysis of first row transition metals, oxides and hydroxides: Cr, Mn, Fe, Co and Ni. Appl. Surf. Sci. *257*, 2717–2730.

Cao, W., Liu, Y., Xu, F., Li, J., Li, D., Du, G., and Chen, N. (2019). In situ electrochemical synthesis of rod-like Ni-MOFs as battery-type electrode for high performance hybrid supercapacitor. J. Electrochem. Soc. *167*, 050503.

Conway, B.E. (1999). Electrochemical Supercapacitors: Scientific Fundamentals and Technological Applications (Plenum Press).

Deng, T., Lu, Y., Zhang, W., Sui, M.L., Shi, X.Y., Wang, D., and Zheng, W.T. (2018). Inverted design for high-performance supercapacitor via Co(OH)(2)-Derived highly oriented MOF electrodes. Adv. Energy Mater. *8*, 1702294.

Deng, T., Zhang, W., Arcelus, O., Kim, J.G., Carrasco, J., Yoo, S.J., Zheng, W., Wang, J., Tian, H., Zhang, H., et al. (2017). Atomic-level energy storage mechanism of cobalt hydroxide electrode for pseudocapacitors. Nat. Commun. *8*, 15194.

Duan, J., Li, Y., Pan, Y., Behera, N., and Jin, W. (2019). Metal-organic framework nanosheets: an emerging family of multifunctional 2D materials. Coord. Chem. Rev. *395*, 25–45.

Furukawa, H., Cordova, K.E., O'Keeffe, M., and Yaghi, O.M. (2013). The chemistry and applications of metal-organic frameworks. Science *341*, 1230444.

Grace Victoria, S., and Moses Ezhil Raj, A. (2018). A systematic probe in the properties of spray coated mixed spinel films of cobalt and manganese. J. Phys. Chem. Sol. *112*, 262–269.

Guan, B., Li, Y., Yin, B., Liu, K., Wang, D., Zhang, H., and Cheng, C. (2017). Synthesis of hierarchical NiS microflowers for high performance asymmetric supercapacitor. Chem. Eng. J. *308*, 1165–1173.

Jiao, Y., Pei, J., Chen, D., Yan, C., Hu, Y., Zhang, Q., and Chen, G. (2017). Mixed-metallic MOF based electrode materials for high performance hybrid supercapacitors. J. Mater. Chem. A *5*, 1094–1102.

Lee, G., Lee, S., Oh, S., Kim, D., and Oh, M. (2020). Tip-to-middle anisotropic MOF-on-MOF growth with a structural adjustment. J. Am. Chem. Soc. *142*, 3042–3049.

Li, H.B., Yu, M.H., Wang, F.X., Liu, P., Liang, Y., Xiao, J., Wang, C.X., Tong, Y.X., and Yang, G.W. (2013). Amorphous nickel hydroxide nanospheres with ultrahigh capacitance and energy density as electrochemical pseudocapacitor materials. Nat. Commun. *4*, 1893.

Li, S.L., and Xu, Q. (2013). Metal-organic frameworks as platforms for clean energy. Energy Environ. Sci. *6*, 1656–1683.

Li, W.H., Ding, K., Tian, H.R., Yao, M.S., Nath, B., Deng, W.H., Wang, Y.B., and Xu, G. (2017). Conductive metal-organic framework nanowire array electrodes for high-performance solid-state supercapacitors. Adv. Funct. Mater. *27*, 1702067.

Liu, Y., Wang, Y., Wang, H., Zhao, P., Hou, H., and Guo, L. (2019). Acetylene black enhancing the electrochemical performance of NiCo-MOF nanosheets for supercapacitor electrodes. Appl. Surf. Sci. *492*, 455–463.

Nam, K.W., Park, S.S., dos Reis, R., Dravid, V.P., Kim, H., Mirkin, C.A., and Stoddart, J.F. (2019). Conductive 2D metal-organic framework for high-performance cathodes in aqueous rechargeable zinc batteries. Nat. Commun. *10*, 4948.

Rajak, R., Saraf, M., Mohammad, A., and Mobin, S.M. (2017). Design and construction of a ferrocene based inclined polycatenated Co-MOF for supercapacitor and dye adsorption applications. J. Mater. Chem. A *5*, 17998–18011.

Severson, K.A., Attia, P.M., Jin, N., Perkins, N., Jiang, B., Yang, Z., Chen, M.H., Aykol, M., Herring, P.K., Fraggedakis, D., et al. (2019). Data-driven prediction of battery cycle life before capacity degradation. Nat. Energy *4*, 383–391.

Sheberla, D., Bachman, J.C., Elias, J.S., Sun, C.J., Shao-Horn, Y., and Dinca, M. (2017). Conductive MOF electrodes for stable supercapacitors with high areal capacitance. Nat. Mater. *16*, 220–224.

Simon, P., Gogotsi, Y., and Dunn, B. (2014). Where do batteries end and supercapacitors begin? Science *343*, 1210–1211.

Sun, P., Ma, R., Bai, X., Wang, K., Zhu, H., and Sasaki, T. (2017). Single-layer nanosheets with exceptionally high and anisotropic hydroxyl ion conductivity. Sci. Adv. *3*, e1602629.

Sun, S., Huang, M., Wang, P., and Lu, M. (2019). Controllable hydrothermal synthesis of Ni/Co MOF as hybrid advanced electrode materials for

supercapacitor. J. Electrochem. Soc. *166*, A1799–A1805.

Talin, A.A., Centrone, A., Ford, A.C., Foster, M.E., Stavila, V., Haney, P., Kinney, R.A., Szalai, V., El Gabaly, F., Yoon, H.P., et al. (2014). Tunable electrical conductivity in metal-organic framework thin-film devices. Science *343*, 66–69.

Wang, L., Feng, X., Ren, L.T., Piao, Q.H., Zhong, J.Q., Wang, Y.B., Li, H.W., Chen, Y.F., and Wang, B. (2015). Flexible solid-state supercapacitor based on a metal-organic framework interwoven by electrochemically-deposited PANI. J. Am. Chem. Soc. *137*, 4920–4923.

Wang, L., Han, Y.Z., Feng, X., Zhou, J.W., Qi, P.F., and Wang, B. (2016). Metal-organic frameworks for energy storage: batteries and supercapacitors. Coordin. Chem. Rev. *307*, 361–381.

Wang, J., Zhong, Q., Xiong, Y., Cheng, D., Zeng, Y., and Bu, Y. (2019a). Fabrication of 3D Co-doped Ni-based MOF hierarchical micro-flowers as a high-performance electrode material for supercapacitors. Appl. Surf. Sci. *483*, 1158–1165.

Wang, Y., Liu, Y., Wang, H., Liu, W., Li, Y., Zhang, J., Hou, H., and Yang, J. (2019b). Ultrathin NiCo-MOF nanosheets for high-performance supercapacitor electrodes. ACS Appl. Energy Mater. *2*, 2063–2071.

Wei, T., Zhang, M., Wu, P., Tang, Y.J., Li, S.L., Shen, F.C., Wang, X.L., Zhou, X.P., and Lan, Y.Q. (2017). POM-based metal-organic framework/reduced graphene oxide nanocomposites with hybrid behavior of battery-supercapacitor for superior lithium storage. Nano Energy *34*, 205–214.

Wen, P., Gong, P., Sun, J., Wang, J., and Yang, S. (2015). Design and synthesis of Ni-MOF/CNT composites and rGO/carbon nitride composites for an asymmetric supercapacitor with high energy and power density. J. Mater. Chem. A *3*, 13874–13883.

Yang, C., Li, X., Yu, L., Liu, X., Yang, J., and Wei, M. (2020). A new promising Ni-MOF superstructure for high-performance supercapacitors. Chem. Commun. (Camb.) *56*, 1803–1806.

Yang, J., Xiong, P.X., Zheng, C., Qiu, H.Y., and Wei, M.D. (2014a). Metal-organic frameworks: a new promising class of materials for a high performance supercapacitor electrode. J. Mater. Chem. A *2*, 16640–16644.

Yang, J., Zheng, C., Xiong, P.X., Li, Y.F., and Wei, M.D. (2014b). Zn-doped Ni-MOF material with a high supercapacitive performance. J. Mater. Chem. A *2*, 19005–19010.

Yoo, J.J., Balakrishnan, K., Huang, J.S., Meunier, V., Sumpter, B.G., Srivastava, A., Conway, M., Reddy, A.L.M., Yu, J., Vajtai, R., and Ajayan, P.M. (2011). Ultrathin planar graphene supercapacitors. Nano Lett. *11*, 1423–1427.

Yuan, M., Wang, R., Fu, W., Lin, L., Sun, Z., Long, X., Zhang, S., Nan, C., Sun, G., Li, H., and Ma, S. (2019). Ultrathin two-dimensional metal–organic framework nanosheets with the inherent open active sites as electrocatalysts in aprotic Li–O2 batteries. ACS Appl. Mater. Interfaces *11*, 11403–11413.

Zhang, J., Fang, J., Han, J., Yan, T., Shi, L., and Zhang, D. (2018). N, P, S co-doped hollow carbon polyhedra derived from MOF-based core–shell nanocomposites for capacitive deionization. J. Mater. Chem. A *6*, 15245–15252.

Zhang, C., Zhang, W., Yu, S.S., Wang, D., Zhang, W.J., Zheng, W.T., Wen, M., Tian, H.W., Huang, K.K., Feng, S.H., and Bentzen, J.J. (2017). Unlocking the electrocatalytic activity of chemically inert amorphous carbon-nitrogen for oxygen reduction: discerning and refactoring the chaotic bonds. Chemelectrochem *4*, 1268.

Zhou, S., Kong, X., Zheng, B., Huo, F., Stromme, M., and Xu, C. (2019). Cellulose nanofiber @ conductive metal-organic frameworks for high-performance flexible supercapacitors. ACS Nano *13*, 9578–9586.

iScience, Volume *23*

Supplemental Information

In-plane Assembly of Distinctive 2D MOFs with Optimum Supercapacitive Performance

Ting Deng, Xiaoyuan Shi, Wei Zhang, Zizhun Wang, and Weitao Zheng

Supporting Information

In-plane Assembly of Distinctive 2D MOFs with Optimum Supercapacitive Performance

Ting Deng, Xiaoyuan Shi, Wei Zhang, Zizhun Wang, and Weitao Zheng

Transparent Methods

Synthesis of $Co(OH)_2$. $Co(OH)_2$ was synthesized by electrochemical deposition method, in which a carbon fiber paper (CFP) was utilized as the substrate. Firstly, CFP was ultrasonically washed with acetone, ethanol and distilled water for 30 min, respectively. After drying, CFP was put in an aqueous solution containing 0.1 M $Co(NO_3)_2$. The electrochemical deposition proceeded at the potential of -0.9 V for 30 min. After the deposition, the prepared $Co(OH)_2$ was rinsed with distilled water and dried at 60℃ overnight. The average mass loading of $Co(OH)_2$ on CFP is ≈ 1.5 mg.

Synthesis of Ni-MOF-24, Co-MOF-24 and Ni MOF array. Ni-MOF-24 was synthesized through a solvothermal method. Typically, 1 mmol of p-benzenedicarboxylic (PTA, ≥99%, Sinopharm Chemical Reagent Co., Ltd.) and 1.5 mmol of nickel nitrate hexahydrate ($Ni(NO_3)_2·6H_2O$, AR, ≥98.0%, Sinopharm Chemical Reagent Co., Ltd.) were dissolved in 20 ml N, N-dimethylformamide (DMF, ≥99.5%, Sinopharm Chemical Reagent Co., Ltd.) in a vial with a capacity of 50 ml. Then we added 2 mL 0.4 M NaOH solution drop by drop. After stirring at room temperature for 30 min, the vial was kept at 120℃ for 24 h. After cooling to room temperature, the light green product was washed with DMF three times. The precipitates were dried at 60 ℃ overnight and herein, then Ni-MOF-24 was obtained. Co-MOF-24 was obtained through the same procedure, with only replacing $Ni(NO_3)_2·6H_2O$ with $Co(NO_3)_2·6H_2O$. Ni MOF array was obtained through the following means: $Co(OH)_2$ was put into the mixture of Ni-MOF-24 precursors. The vial was kept at 120℃ for 12h. After cooling to room temperature, CFP was washed with ethanol and DMF for several time and dried in a 60 ℃ oven overnight. The average mass loading of Ni MOF array on CFP was ≈ 2 mg.

Synthesis of $Cu_3(HITP)_2$. $Cu_3(HITP)_2$ was synthesized through a solvothermal method. Solution A: 20 mL ethanol containing 64 mg $Cu(NO_3)_2$ ($Cu(NO_3)_2$, AR, ≥98.0%, Sinopharm Chemical Reagent Co., Ltd.); Solution B: 30 mL ethanol containing 52 mg 2,3,6,7,10,11-hexaaminotriphenylene hexaphydrochloride (HITP·6HCl). Then solution A and B was mixed and stirred for 30 mins. After that the mixed solution was transferred to a vial of 50 ml, which was put in a 65℃ oven for 24 h. After cooling to room temperature, the dark blue product was washed with DMF three times. Then the precipitates were dried at 60 ℃ overnight and herein, the $Cu_3(HITP)_2$ was obtained.

Synthesis of Ni//Cu MOF array and powder. A small amount of $Cu(NO_3)_2$ (48 mg) and HITP ligand (39 mg) were added into the precursors of Ni-MOF-24. After stirring for 30 mins, $Co(OH)_2$/CFP electrode was put into the vial. Then the vial was transferred to a 120℃ oven for 12 h. After cooling down to room temperature, CFP was washed with ethanol and DMF for several time and dried in a 60 ℃ oven overnight. The average mass loading of Ni//Cu MOF array on CFP was ≈ 2 mg. And the precipitate was washed with DMF three times dried at 60 ℃ overnight. Co//Cu MOF powder was obtained through

the same procedure.

Synthesis of working electrodes. Co//Cu MOF, Co MOF and active carbon (AC) electrodes were fabricated using a method as follows: a mixture of active material, acetylene, nafion (wt.%: 85:10:5) and a small amount of ethanol were prepared by stirring 6 h to produce a homogeneous paste. This paste was pressed onto CFP to yield working electrode. The average mass loading of Co//Cu MOF and Co MOF is ~ 2 mg, and AC is ~ 3 mg.

Physical characterization. Surface morphology of the prepared electrodes was studied by using scanning electron microscopy (SEM, a Hitachi SU8010 scanning electron microscope operated at 2 kV). High-angle annular dark field (HAADF)-STEM image and energy dispersive X-ray (EDS) elemental maps were obtained by a transmission electron microscope (TEM, JEM-2100F). The structural information was investigated using X-ray diffraction (XRD) (RIGAKU D/MAX2500, λ=1.54 nm). Surface states of materials were studied by X-ray photoelectron spectroscopy (XPS, ESCALAB-250 performed with a monochromatic Al Kα radiation source and a hemisphere detector with an energy resolution of 0.1 eV).

Electrochemical evaluation. Electrochemical measurements were carried out on a computer-controlled potentiostat (CHI660E, CH instrument, Shanghai) with a three-electrode electrochemical cell containing aqueous solution as electrolyte. A platinum plate and a saturated calomel electrode (SCE) were used as counter electrode and reference electrode, respectively. The electrolyte (1 M KOH) was prepared from high purity KOH pellets (AR, ≥85.0%, Sinopharm Chemical Reagent Co., Ltd.) by adding 56 g of pellets to 1 L distilled water. A two-electrode cell configuration was used to measure the performance of hybrid supercapacitor in 1 M KOH aqueous electrolyte solution. The working electrodes were placed together and separated by a porous non-woven cloth separator. Then cyclic voltammetry was used to investigate its activity. Its charge/discharge ability was measured by a galvanostatic test. For the linear behavior, the capacitance is calculated by the equation: $C=(i\times\Delta t)/(m\times\Delta V)$; for the non-linear behavior, the capacitance is calculated using the following equation: $C=2I_m(\int Vdt)/V^2$, where Im is the current density (Mai et al., 2013; Sundriyal et al., 2018). The energy and power densities of the asymmetric capacitor were calculated as follow: $E=0.5\times C\times V^2$, $P=I\times V/m$, where E (Wh Kg^{-1}) denotes the energy density, and P (W kg^{-1}) represents the power density.

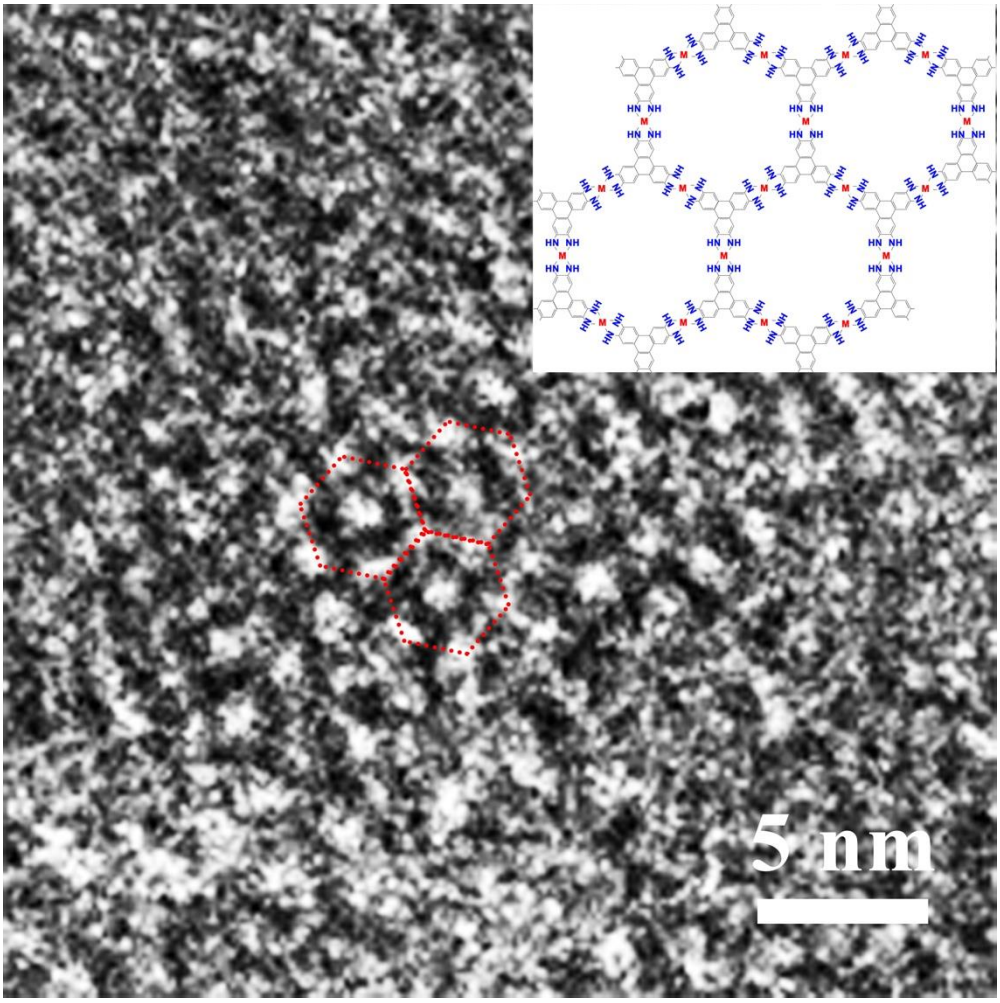

Figure S1. HRTEM image of $Cu_3(HITP)_2$ shows a honeycomb pore structure with a perfect hexagonal arrangement of lattices. The inset is the 2D chemical structure of $Cu_3(HITP)_2$ and the unit cell parameters are $a = b = 22.3$ Å and $c = 6.6$ Å. Related to Figure 1.

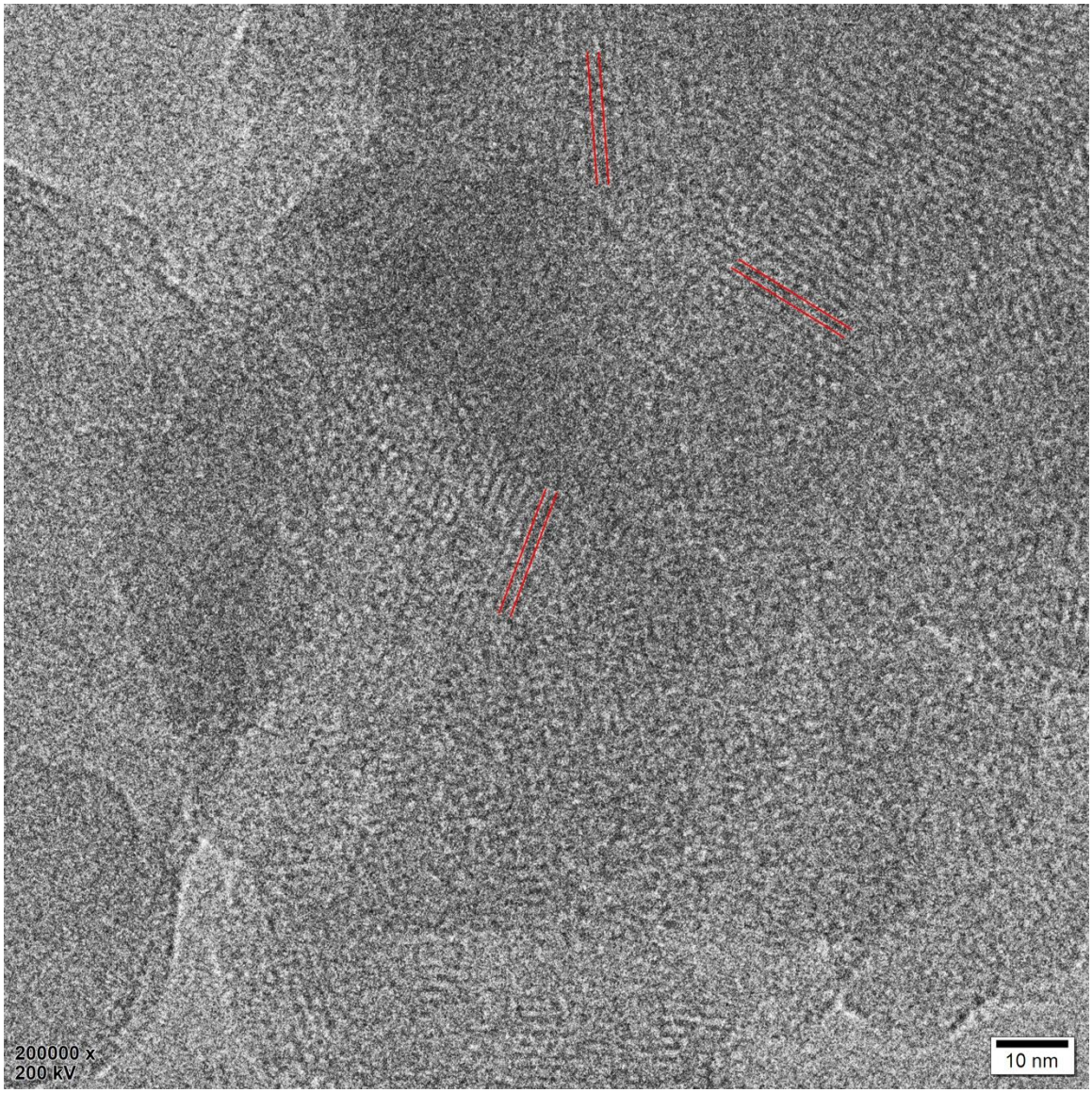

Figure S2. HRTEM image of $Cu_3(HITP)_2$ and the lattice fringe is calculated to be 0.92 nm, in accordance with the d_{100}-spacing of $Cu_3(HITP)_2$. Related to Figure 1.

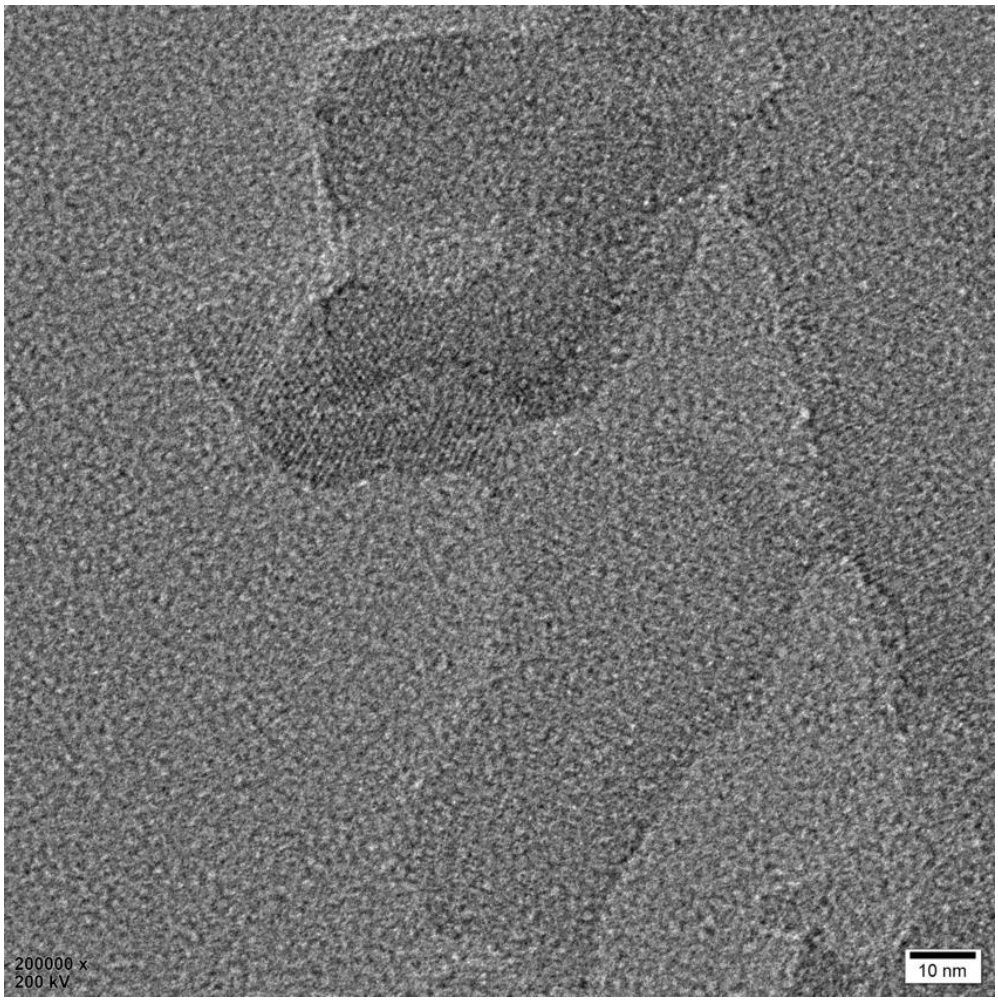

Figure S3. HRTEM image of Ni//Cu MOF indicates this MOF//MOF strategy preserves the original layer structure of Ni-MOF-24 and $Cu_3(HITP)_2$. Related to Figure 1.

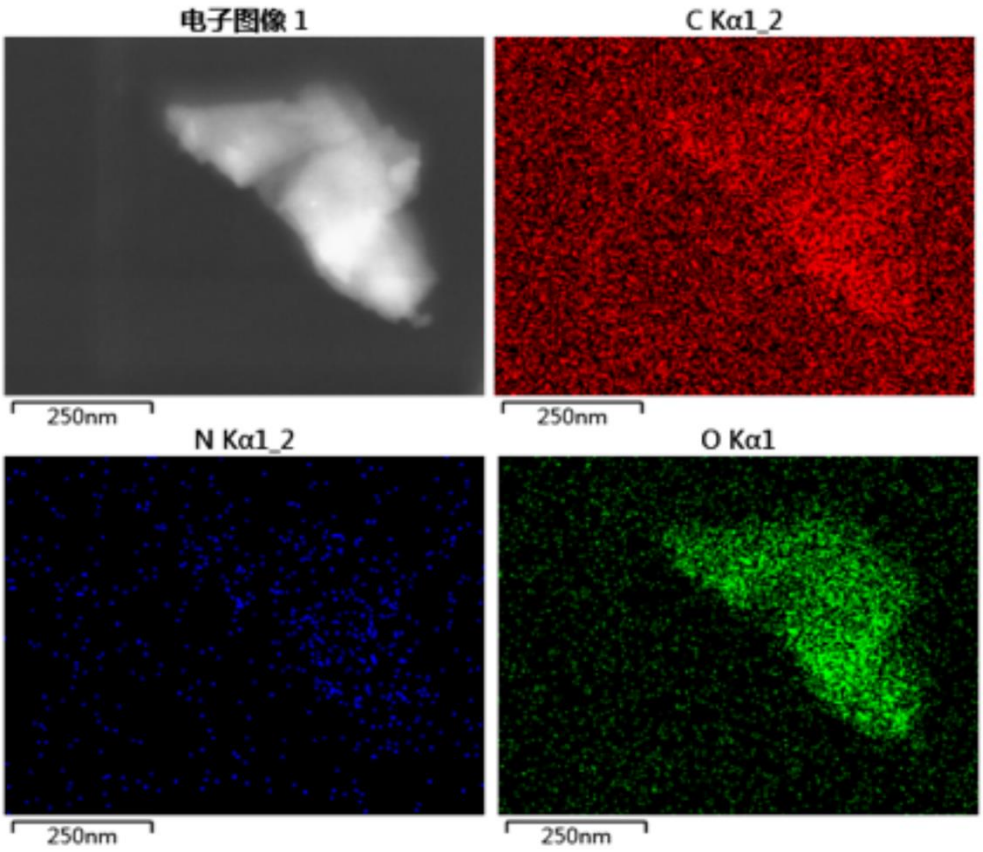

Figure S4. EDS elemental mapping of C, N and O in Ni//Cu MOF. Related to Figure 2.

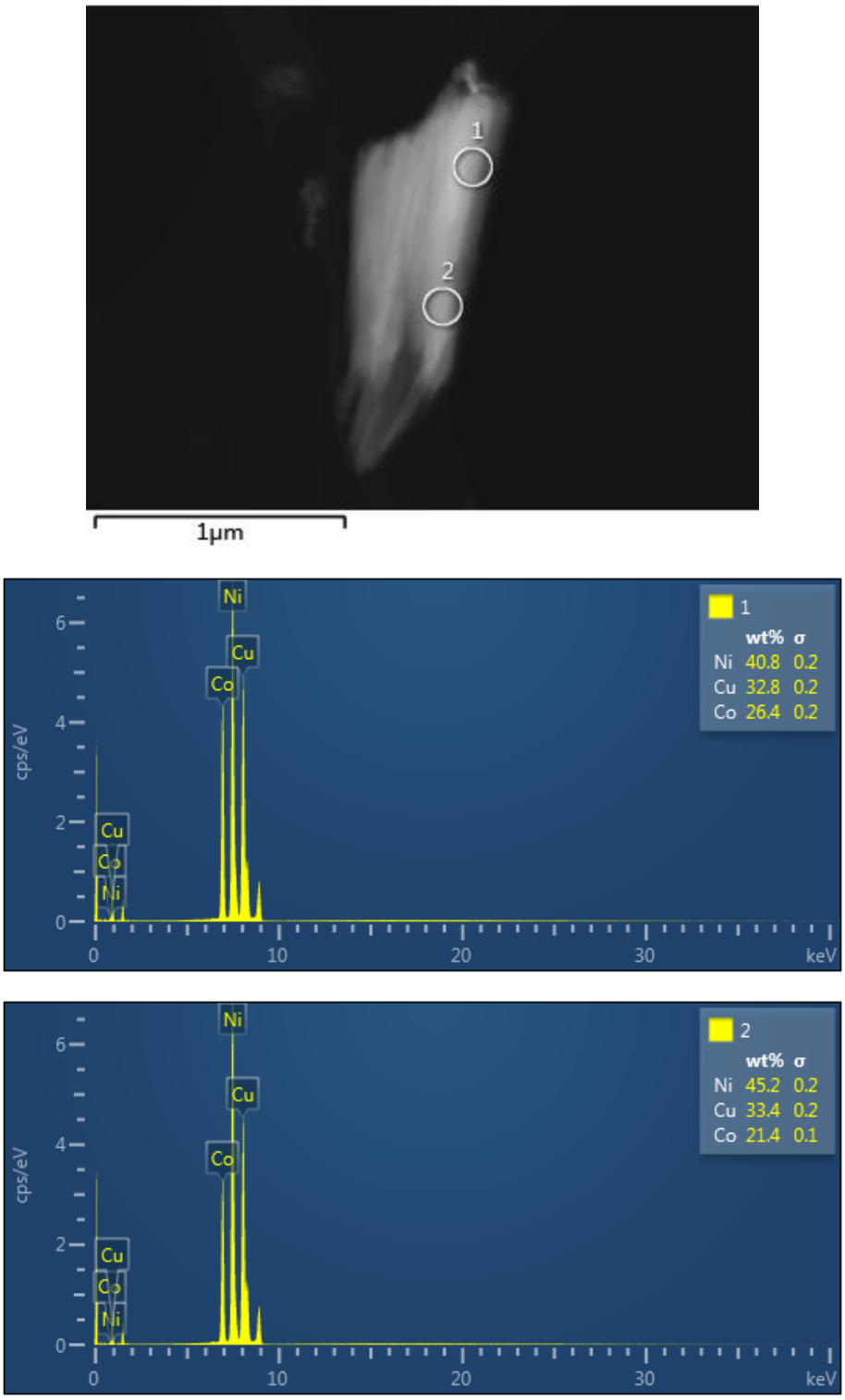

Figure S5. EDX spectra of Ni//Cu MOF array on CFP. The contents 1 and 2 corresponds to the circled areas in the SEM image. Related to Figure 2.

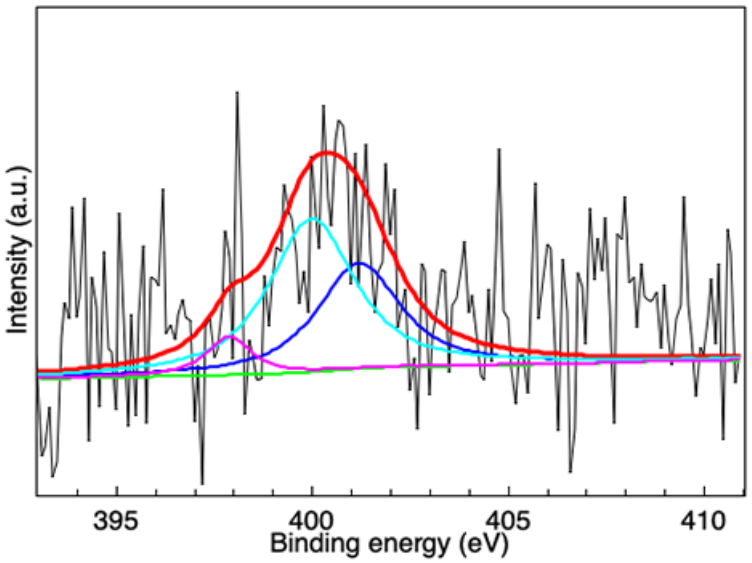

Figure S6. XPS spectrum of N in Ni//Cu MOF. Related to Figure 2.

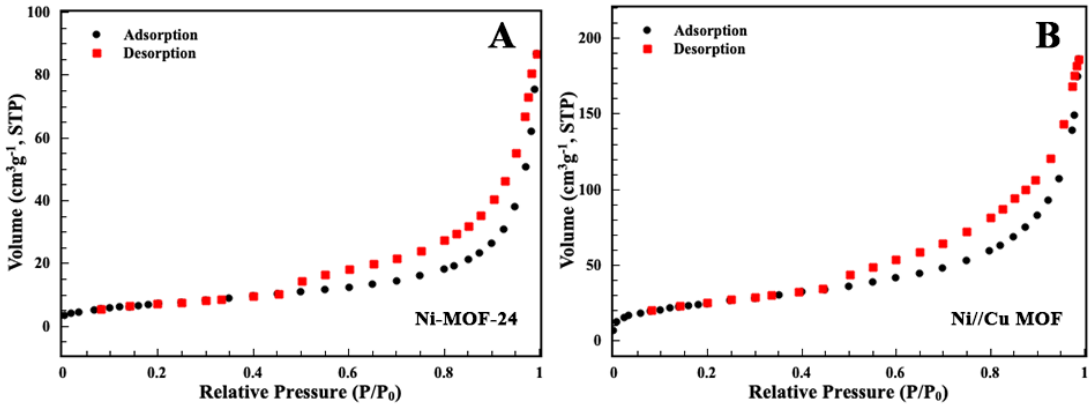

Figure S7. N_2 isotherm tests for A, Ni-MOF-24. B. Ni//Cu MOF. The SSA is 26 and 90 m^2g^{-1}, respectively. Related to Figure 2.

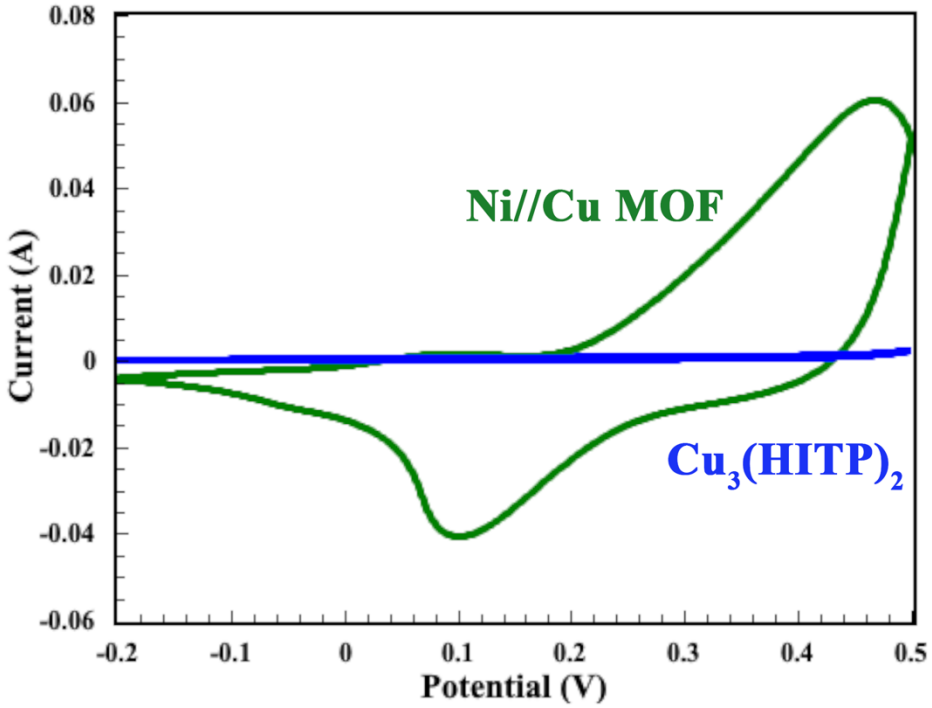

Figure S8. CV curves of $Cu_3(HITP)_2$ and Ni//Cu MOF collected at the scan rate of 10 mVs^{-1}. Related to Figure 3.

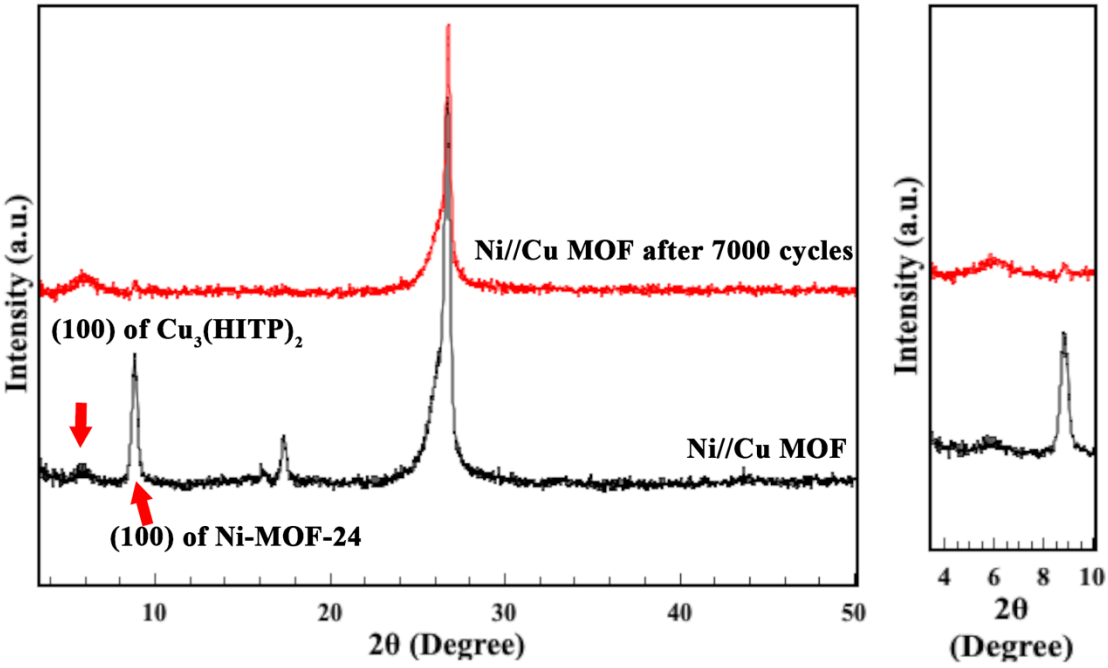

Figure S9. XRD patterns of uncycled Ni//Cu MOF and Ni//Cu MOF after 7000 cycles. Related to Figure 3.

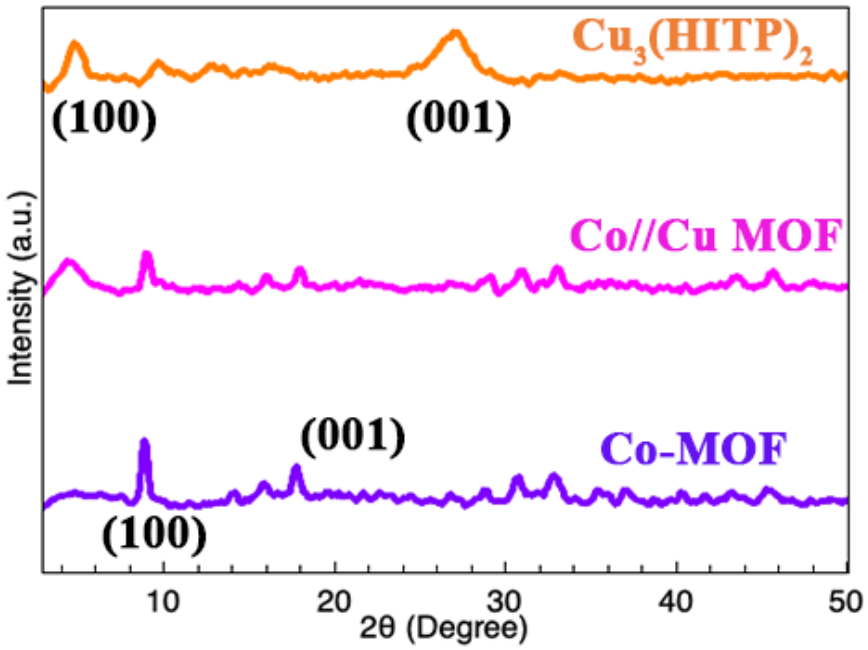

Figure S10. XRD patterns of Co-MOF, $Cu_3(HITP)_2$ and Co//Cu MOF. Co//Cu MOF also shows the peak centered around 5 degrees which belongs to $Cu_3(HITP)_2$ while the peak at 27 degrees of $Cu_3(HITP)_2$ disappears, indicating the successful fusion of two layered MOFs. Related to Figure 1.

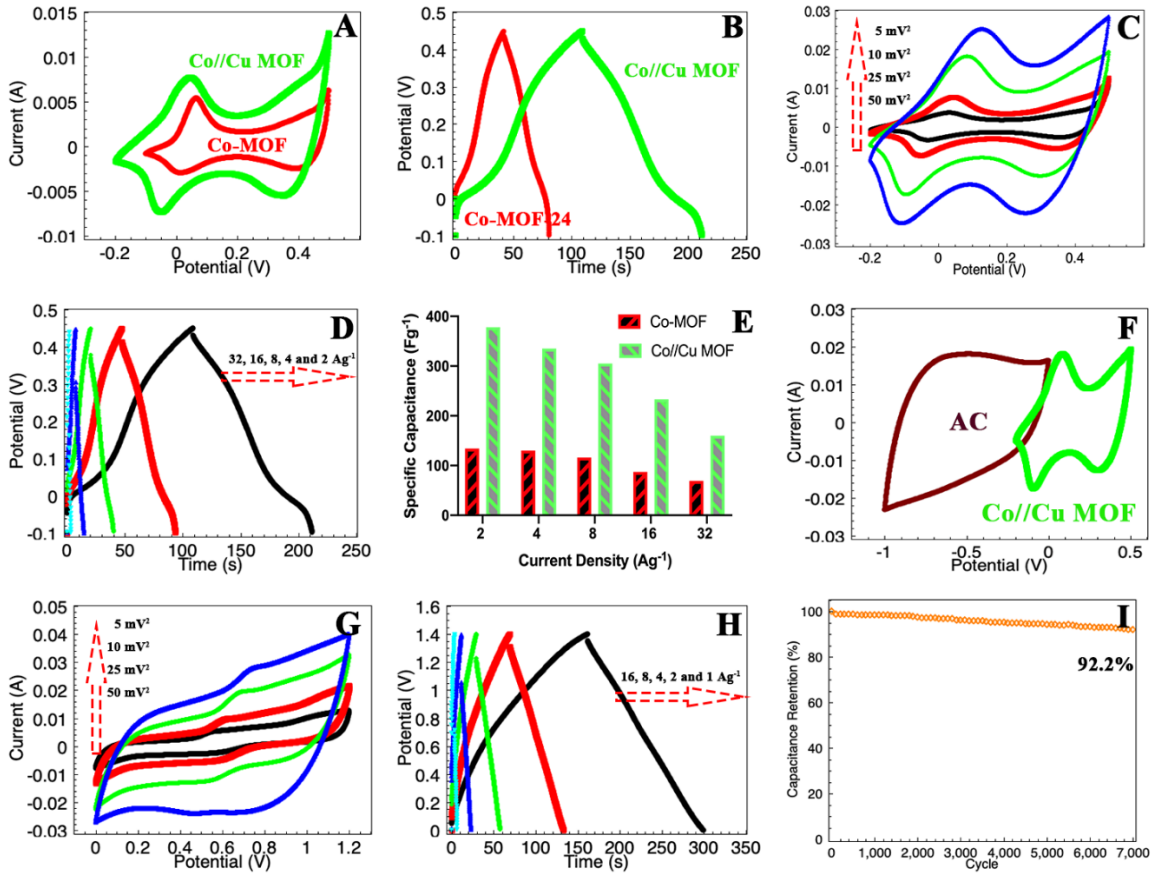

Figure S11. Electrochemical evaluation of Co//Cu MOF and the corresponding hybrid supercapacitor. **A**. CV curves of Co-MOF and Co//Cu MOF at the scan rate of 10 mVs^{-1}. **B**, Charge/discharge profiles of Co-MOF and Co//Cu MOF at the current density of 2 Ag^{-1}. The capacitance can reach 134 and 378 Fg^{-1}, respectively. **C**. CV curves of Co//Cu MOF at the scan rate ranging from 5 to 50 mVs^{-1}. **D**. Charge/discharge profiles of Co//Cu MOF at the current of 2, 4, 8, 16 and 32 Ag^{-1}, respectively. The specific capacitance can reach 378, 335, 305, 233 and 160 Fg^{-1}, respectively. **E**. The capacitance comparison between Co-MOF and Co//Cu MOF at different current densities. **F**. CV curves of AC and Co//Cu MOF at the scan rate of 25 mVs^{-1}. **G**. CV curves of hybrid supercapacitor collected at different scan rates. **H**. Charge/discharge profiles of hybrid supercapacitor collected at different current densities. **I**. The stability of the capacitor. After 7000 cycles, the capacitance holds a 92.2 % retention of its initial capacitance. Related to Figures 3 and 4.

Supplemental References

Mai, L.-Q., Minhas-Khan, A., Tian, X., Hercule, K. M., Zhao, Y.-L., Lin, X. and Xu, X. (2013). Synergistic interaction between redox-active electrolyte and binder-free functionalized carbon for ultrahigh supercapacitor performance. Nat. Commun., *4*, 2923.

Sundriyal, S., Shrivastav, V., Kaur, H., Mishra, S. and Deep, A. (2018). High-Performance Symmetrical Supercapacitor with a Combination of a ZIF-67/rGO Composite Electrode and a Redox Additive Electrolyte. ACS Omega, *3*, 17348-17358.